Magainin 2 Amide Interaction with Lipid Membranes: Calorimetric Detection of Peptide Binding and Pore Formation†

Markus R. Wenk‡ and Joachim Seelig*

Department of Biophysical Chemistry, Biocenter of the University of Basel, Klingelbergstrasse 70, CH-4056 Basel, Switzerland

Received October 22, 1997; Revised Manuscript Received January 8, 1998

ABSTRACT: The interaction of the antibiotic magainin 2 amide (M2a) with lipid bilayers was investigated with high-sensitivity titration calorimetry. The enthalpy of transfer of the cationic M2a to negatively charged small unilamellar vesicles composed of 1-palmitoyl-2-oleoyl-*sn*-glycero-3-phosphocholine (POPC) and 1-palmitoyl-2-oleoyl-*sn*-glycero-3-phosphoglycerol (POPG) (75:25, mol/mol) was measured as $\Delta H = -17.0 \pm 1$ kcal/mol of peptide. The adsorption isotherm was determined by injecting lipid vesicles into peptide solutions at low peptide concentrations ($c_P^o < 7\ \mu$M). The apparent partition coefficient was $K_{app} \approx 1.2 \times 10^4\ M^{-1}$ at a peptide equilibrium concentration of 1 μM but decreased with increasing peptide concentration. The hydrophobic partitioning of M2a into the lipid membrane is modulated by electrostatic effects that arise from the attraction of the positively charged peptide to the negatively charged membrane. Using the Gouy−Chapman theory to correct for electrostatic attraction, the experimental binding isotherms can be explained with an intrinsic (hydrophobic) partition coefficient of $K = 55 \pm 5\ M^{-1}$ and an effective peptide charge of $z = 3.7-3.8$. The free energy of binding is $\Delta G = -4.8$ kcal/mol. At peptide concentrations $c_P^o > \sim 7\ \mu$M, a second effect comes into play, and the titration enthalpies can no longer be explained exclusively by peptide partitioning. The first few injections produce enthalpies of reaction which are distinctly smaller than expected from a pure partition equilibrium, followed by a series of injections with reaction heats larger than expected. After subtracting the enthalpic contribution due to partitioning, the residual enthalpies are endothermic for the first few injections, and exothermic for the consecutive steps. Furthermore, the endothermic excess heat is compensated exactly by the exothermic excess heat; i.e., the excess heat consumed in the first part of the titration experiment is returned during the second part. Endothermic excess enthalpies are observed for total molar peptide-to-lipid ratios of P/L > ∼3.0%, whereas exothermic excess heats were seen for 0.7% < P/L < 3.0%. Below P/L < ∼0.7%, the binding follows the partition equilibrium. Based on earlier spectroscopic evidence, it is suggested that magainin 2 amide binds to the lipid membrane and forms pores at high peptide-to-lipid ratio, this process being characterized by an endothermic reaction enthalpy. Pore formation is reversed with increasing lipid concentration, and the peptide pores disintegrate. The limiting peptide-to-lipid ratio deduced from titration calorimetry for M2a pore formation is in excellent agreement with spectroscopic methods. The enthalpy of pore formation amounts to $\Delta H = +6.2 \pm 1.6$ kcal/mol peptide or $\Delta H \sim 25-45$ kcal/mol pore if the pore is comprised of 4−7 peptide molecules.

Magainins are a class of antimicrobial peptides which are secreted from the skin of *Xenopus laevis* (*1, 2*). They are bacteriocidal, fungicidal, and virucidal but not hemolytic and are therefore of pharmaceutical interest as broad-band antibiotics. Magainins were also found to act selectively against a number of tumor cell lines, making them potential candidates for anti-cancer therapies with low side-effects (*3, 4*). Magainins consist of 21−26 amino acid residues and are highly positively charged (+3 to +5). At physiological pH, they are soluble in aqueous solutions at high concentrations. Magainins show secondary structural homology to lytic peptides isolated from bee and wasp venoms and have been classified as class L amphipathic α-helices (*5*). In the helical conformation, they possess a large hydrophobic moment, a broad nonpolar face, and a narrow polar face; the positive charges of the lysine residues are clustered at the border of the polar/nonpolar face (*5, 6*). Due to their ability to form an amphipathic helix, magainins show a high tendency to bind to lipid membranes [for a recent review, see (*7*)]. Membrane binding may be accompanied by a perturbation of the bilayer (*8, 9*). The cytotoxic effects of magainins are thought to arise from a permeabilization of the cell membrane (*10−12*), though the mechanism and selectivity of action are a matter of current debate (*7, 13−15*).

Magainin 2 and its derivatives are by far the most intensely investigated members of the magainin family. Their interaction with membranes was shown to be strongly promoted by the presence of negatively charged lipids (*11, 16*). Furthermore, magainin 2 was shown to induce efflux of water-soluble molecules encapsulated in artificial membranes

† Supported by Swiss National Science Foundation Grant 31.42058.94.

* Address corresspondence to this author. Telephone: +41-61-267-2190. Fax: +41-61-267-2189. E-Mail: Seelig1@ubaclu.unibas.ch.

‡ Present address: Department of Cell Biology, Yale University School of Medicine, New Haven, CT 06510.

S0006-2960(97)02615-9 CCC: $15.00
Published on Web 02/24/1998

(*11*, *17*), to form ion channels in planar lipid membranes (*18*, *19*), and to dissipate the electrochemical proton gradient across lipid bilayers (*10*, *12*). The structure and orientation of the magainin molecules in the membrane leading to these effects have been investigated by circular dichroism (*20*), nuclear magnetic resonance (*21*−*23*), Raman spectroscopy (*24*), and fluorescence spectroscopy (*25*), as well as neutron in-plane scattering (*14*). At a low peptide-to-lipid ratio, the peptide molecules were shown to be in a helical conformation, located in the lipid headgroup region and aligned essentially parallel to the bilayer surface (*20*, *22*, *23*, *26*). At higher peptide-to-lipid ratios, an orientation perpendicular to the bilayer surface was suggested by circular dichroism spectroscopy (*20*). A torroidal arrangement of magainin molecules (in a helical conformation) inserted in a distorted lipid bilayer has been proposed where the inner and outer leaflets are fused (*14*, *27*, *28*). The transition from a parallel to a perpendicular orientation (with respect to the bilayer surface) occurs at concentrations similar to those required for cytolytic activity (*10*, *12*).

In this study, we used high-sensitivity titration calorimetry to investigate the binding of magainin 2 amide (M2a) to unilamellar phospholipid vesicles composed of 1-palmitoyl-2-oleoyl-*sn*-glycero-3-phosphocholine (POPC) and 1-palmitoyl-2-oleoyl-*sn*-glycero-3-phosphoglycerol (POPG) (75:25, mol/mol). We measured the enthalpy of M2a partitioning into the lipid membrane as well as the binding isotherm. At low peptide concentrations, the latter could be described quantitatively by a combination of the Gouy−Chapman theory (correcting for electrostatic effects) and a simple surface partition equilibrium, characterized by an intrinsic (hydrophobic) partition coefficient. These results provided a full thermodynamic description of M2a binding to negatively charged lipid membranes. For peptide concentrations above $c_P^o \approx 7$ μM, the titration curves exhibited a more complex behavior. From a series of experiments with different peptide concentrations, a partial "phase diagram" of the lipid/peptide system could be constructed from the titration isotherms. The boundaries separating the regions correlate with data reported for pore formation and cyctotoxic activity, respectively.

MATERIALS AND METHODS

Materials. Magainin 2 amide (M2a) (GIGKFLHSAKKF-GKAFVGEIMNS-NH_2) was a gift from Magainin Pharmaceuticals Inc. (Plymouth Meeting, PA). The puritiy was checked by mass spectroscopy. 1-Palmitoyl-2-oleoyl-*sn*-glycero-3-phosphocholine (POPC) and 1-palmitoyl-2-oleoyl-*sn*-glycero-3-phosphoglycerol (POPG) were obtained from Avanti Polar Lipids (Birmingham, AL). All chemicals were employed without further purification. Buffers were prepared from 18 MΩ water obtained from a NANOpure A filtration system.

Preparation of Lipid Vesicles. Small unilamellar vesicles (SUV) were prepared as follows. A defined amount of lipid (∼50 mg) was first dried under a stream of nitrogen, followed by high vacuum for 1 h at room temperature and in the dark. The lipid was then dissolved in dichloromethane (0.5 mL) and again dried under nitrogen. High vacuum was applied overnight. A defined amount of buffer (2 mL) was added to the lipid film, and the suspension was vortex-mixed extensively. Next, the lipid dispersions were sonicated for 10−20 min ($T = 10$ °C) until the solution became transparent. The opalescent solution was centrifuged in an Eppendorf table-top centifuge (8 min at 14 000 rpm) to remove metal debris. Lipid concentrations were determined gravimetrically by carefully weighing the samples immediately after drying and by adding defined amounts of buffer (10 mM Tris, 100 mM NaCl, pH 7.4). In separate experiments, we have analyzed the lipid content of sonified vesicles with phosphorus analysis (*29*). The phosphate analysis yielded a 4.7% (average of 9 determinations) smaller lipid content than the nominal concentration, with maximum deviations between −2% and +10%. The data reported were calculated on the basis of the weighing-in concentration.

High-Sensitivity Titration Calorimetry. Isothermal titration calorimetry was performed using an Omega high-sensitivity titration calorimeter from Microcal (Microcal, Northampton, MA) (*30*). Solutions were degassed under vacuum prior to use to eliminate air bubbles. The calorimeter was calibrated electrically. The data were acquired by computer software developed by MicroCal. In control experiments, the corresponding peptide solution (or vesicle suspension) was injected into buffer without lipid (or without peptide). Heats of dilution were small compared to the actual measurement but were nevertheless included in the final analysis.

RESULTS

Binding Enthalpy and Titration Isotherms. We have used high-sensitivity titration calorimetry to investigate the binding of magainin 2 amide (M2a) to phospholipid vesicles. In the first type of experiment, the calorimeter cell contained sonified vesicles composed of POPC and POPG, and small aliquots of M2a were injected. A typical result is shown in Figure 1A. In each step, 4 μL of a 203 μM M2a solution was injected into a suspension of mixed POPC/POPG (75:25, mol/mol) small unilamellar vesicles. The reaction is exothermic, and the heat of reaction is $h_i \approx -14.5$ μcal per injection as derived from the integration of the titration peaks (Figure 1B). In a control experiment, peptide was injected into buffer. The heat of reaction was small (±1.5 μcal/inj) and was indistinguishable from a buffer-into-buffer titration. The heat of M2a partitioning into POPC/POPG membranes, ΔH, can be calculated under the assumption that all injected peptide is bound to the lipid vesicles. The average heat of reaction measured at three different peptide concentrations was $\Delta H = -16.7 \pm 1.1$ kcal/mol.

In a second type of titration experiment, the peptide solution was contained in the calorimeter cell, and lipid vesicles were injected. Figure 2 displays an experiment where 10 μL aliquots of a phospholipid vesicle suspension [POPC/POPG (75:25, mol/mol); total lipid concentration $c_L^o = 27.86$ mM] were injected into the reaction cell ($V = 1.2778$ mL) containing magainin 2 amide ($c_P^o = 6.6$ μM). Each injection produced an exothermic heat of reaction, h_i, which decreased in magnitude with consecutive injections. As a control, buffer without lipid was injected into the peptide solution (data not shown). The heat of dilution, $h_{d,i}$, varied between +1.5 and −1.5 μcal per injection. The heat of dilution was subtracted, and the quantitative evaluation

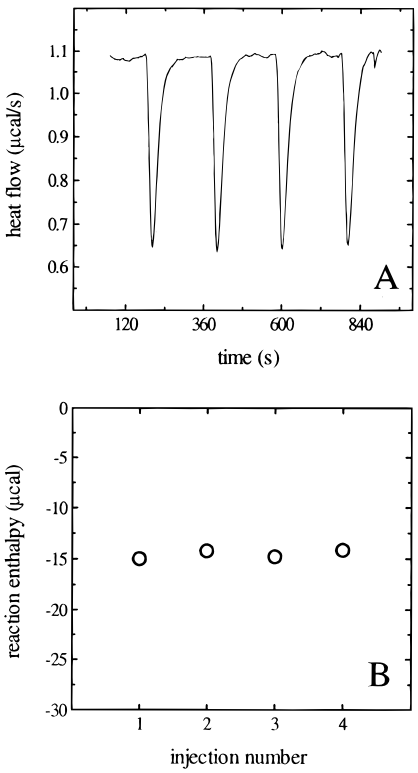

FIGURE 1: Titration calorimetry of small unilamellar vesicles (POPC/POPG, 75:25, mol/mol, c_L= 15.5 mM) with a solution of magainin 2 amide (203 μM). Aliquots (4 μL) of peptide solution were added to the lipid suspension in the reaction cell (V = 1.2778 mL). The reference cell contained buffer (10 mM Tris, pH 7.4, 100 mM NaCl). T = 30 °C. Panel A shows the calorimeter tracing; downward peaks denote exothermic reactions. The heat per injection as evaluated from the areas underneath the tracing is shown in panel B.

of the experimental data was based on

$$\delta h_i = h_i - h_{d,i} \quad (1)$$

The cumulative heat of reaction after i injections

$$\delta H_i = \sum_{k=1}^{i} \delta h_k \quad (2)$$

is shown in Figure 2B. It can be seen from Figure 2 that the reaction has largely ceased after about i = 10 injections of lipid vesicles. At this stage of the experiment, almost all peptide is bound to the lipid vesicles, and the free peptide concentration is small. Addition of more lipid entails no further reaction. The cumulative heat of all injections amounts to $\delta H_{10} = \sum_{k=1}^{10} \delta h_k \approx -149.8\ \mu$cal. Since the total amount of peptide present in this experiment was n_P^o = (1.2778 mL)(6.6 μM) $\approx$ 8.4 nmol, the molar enthalpy of binding amounts to $\Delta H = \delta H_{10}/n_P^o \approx -17.8$ kcal/mol, which is consistent with the value determined in the peptide-into-lipid titrations described above. The good agreement between the two types of experiments provides evidence for a virtually complete binding of M2a in the experiment shown in Figure 1.

Titration curves analogous to that shown in Figure 2 were observed for peptide solutions with concentrations up to $c_P^o \leq 7\ \mu$M. Under these conditions, the titration curve can be explained by a partition equilibrium of M2a modified by electrostatic interactions. It is possible to derive the binding

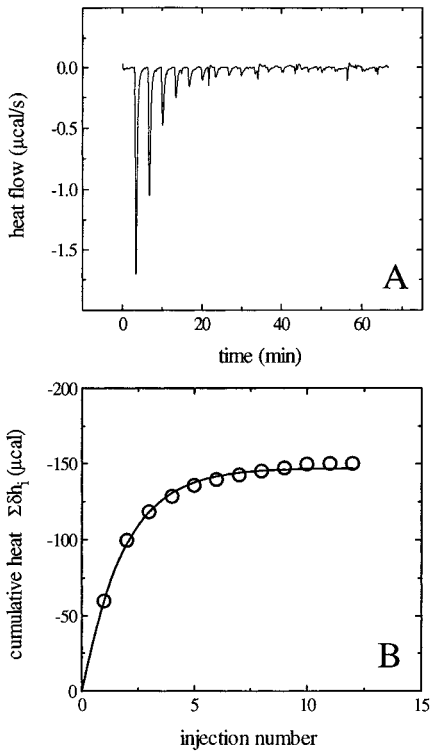

FIGURE 2: Titration calorimetry of a magainin 2 amide solution (6.6 μM) with small unilamellar lipid vesicles (POPC/POPG, 75:25, mol/mol, c_L= 27.86 mM). (A) Each peak corresponds to the injection of 10 μL of lipid suspension into the reaction cell (V = 1.2778 mL) containing the peptide solution. The reference cell contained buffer (10 mM Tris, pH 7.4, 100 mM NaCl). T = 30 °C. (B) Cumulative heat of reaction as a function of the injection number. The solid line was calculated using a surface partition equilibrium of the form $X_b = Kc_M$, where X_b denotes the molar ratio of membrane-bound peptide/total lipid (on the outer vesicle surface) and c_M is the free peptide concentration immediately above the plane of binding. c_M was calculated by means of the Gouy−Chapman theory. The effective peptide charge was z = 3.7−3.8, the intrinsic binding constant K = 50 M^{-1}, and the reaction enthalpy ΔH = −17.7 kcal/mol (cf. text for details). The peptide binding was limited to the outer monolayer of the lipid vesicle (60% of total lipid).

isotherm and to determine the partition constant K as will be discussed below. The solid line in Figure 2B then corresponds to the theoretical titration curve calculated with this model, using a partition (binding) constant of K = 50 M^{-1} and a pH-dependent peptide charge of z = 3.7−3.8. The theoretical analysis further assumes that M2a binds to the outer surface of the bilayer vesicle only (60% of total lipid).

At peptide concentrations larger than 7 μM, more complicated titration patterns were observed (Figure 3A−E). The heat of reaction no longer decreased smoothly with each injection but showed an inflection point. This is particularly obvious when the experimental heats of reaction are compared with the theoretical titration curves. The latter were calculated with essentially the same binding model as used in Figure 2. However, at these higher peptide concentrations, a rapid flip-flop of the lipids combined with a peptide translocation across the membrane was assumed in accordance with recent fluorescence and neutron diffraction studies (*14*, *27*). The rapid lipid exchange requires that all lipid be considered in the calculation of the peptide binding isotherm. During the first few injections, the measured $|\delta h_i|$

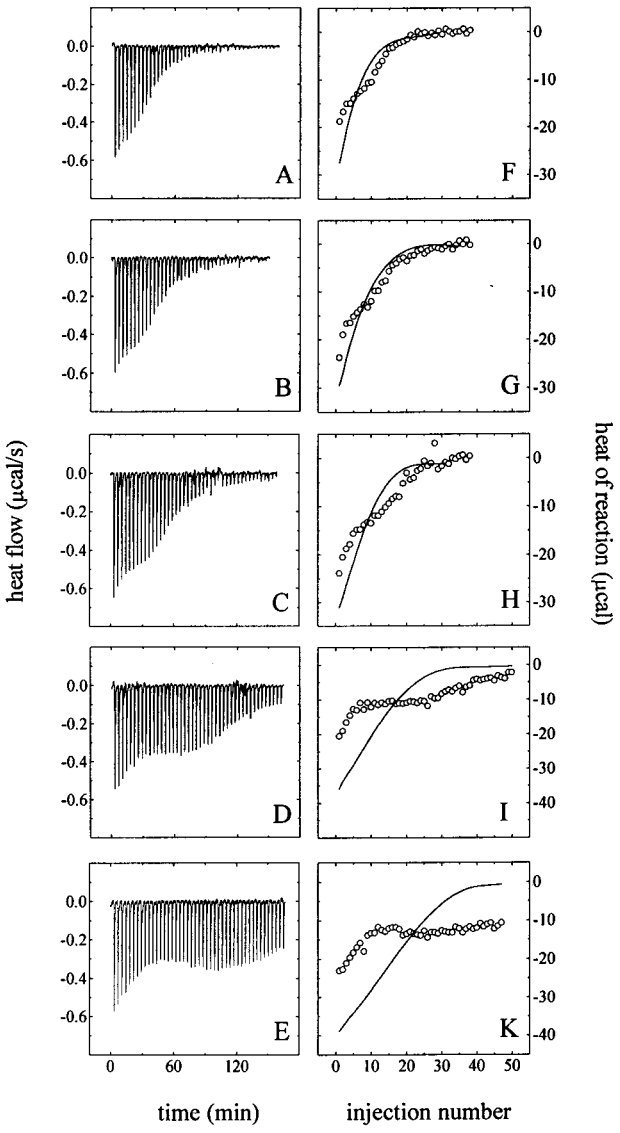

FIGURE 3: Titration calorimetry of magainin 2 amide solutions with sonicated vesicles (POPC/POPG, 75:25, mol/mol). The panels on the left show the calorimeter tracings. In each titration step, 5 μL of lipid suspension ($c_L \approx 10$ mM) was injected into the reaction cell ($V = 1.2778$ mL) containing the peptide solution (the peptide concentrations are increasing from top to bottom). The reference cell contained buffer (10 mM Tris, pH 7.4, 100 mM NaCl). $T = 30$ °C. The specific measuring conditions were as follows: (A) $c_L^o = 12.14$ mM, $c_P^o = 8.26$ μM; (C) $c_L^o = 12.14$ mM, $c_P^o = 10.65$ μM; (E) $c_L^o = 12.14$ mM, $c_P^o = 12.86$ μM; (G) $c_L^o = 12.06$ mM, $c_P^o = 21.8$ μM; (I) $c_L^o = 12.06$ mM, $c_P^o = 31.2$ μM. The panels on the right show the heats of reaction per injection vs the injection number. The open circles are the experimental titration peaks δh_i. The solid lines are the calculated contribution of peptide partitioning as described in the text. The simulation parameters were identical in all cases. $K = 60$ M^{-1}, $\Delta H = -17$ kcal/mol, and $z = 3.7-3.8$, depending on the membrane surface pH. The simulations were performed with the assumption that all phospholipid was available for binding.

are *smaller* than the theoretical expectations. This is followed by an about equal number of injection steps where $|\delta h_i|$ is *larger* than the calculated values. Finally, after a sufficiently large number of injections, the δh_i values follow the theoretical line; i.e., the experimental data correspond to a simple partition model modulated by electrostatic interactions.

An analogous behavior was observed before for the partitioning of the surfactant octyl β-D-glucopyranoside (OG) into lipid membranes (*31*, *32*) and was explained by a second thermodynamic process superimposed on OG partitioning into membranes. This process could be identified by a micelle formation ↔ demicellization equilibrium of the phospholipid/surfactant mixture (*32*). Such a dramatic change can be excluded in the present experiments since the integrity of the lipid vesicles was checked by light scattering experiments (data not shown). In a typical experiment, 10 μL aliquots of a lipid vesicle suspension, equal to that used in the calorimetric titrations, were injected into peptide solutions of different concentrations, and the scattering signal at 90° with respect to the incoming beam was recorded as a function of time. For the peptide concentrations used in these studies, the scattering intensities were equal to the control values (vesicles into buffer without peptide) within experimental accuracy. These results indicate the absence of any peptide-induced disruption of lipid vesicles under the experimental conditions used. The excess heats observed in the present titration experiments can thus not be explained by a micellation process. Instead they are assigned to the formation of membrane pores composed of M2a and lipids as suggested by recent spectroscopic results (*14*, *27*).

The cumulative heat of reaction of all injections shown in Figure 3A amounts to $\delta H = \sum_i \delta h_i = -173$ μcal. The amount of M2a in the calorimeter cell is $n_P^o = 10.6$ nmol, yielding a molar heat of reaction of $\Delta H = -16.4$ kcal/mol. For the experiments displayed in Figure 3B,C, the corresponding values amount to -16.7 kcal/mol and -17.7 kcal/mol, respectively. The results are in excellent agreement with the measurements shown in Figures 1 and 2 and suggest that the loss in δh_i during the first part of the titration (compared to the theoretical titration curve) is returned in the second half.

Binding Isotherms and Apparent Partition Coefficient, K_{app}. The binding isotherm, $X_b = f(c_{P,f})$, provides the functional dependence between peptide bound to the membrane (X_b) and peptide free in solution ($c_{P,f}$). The binding isotherm can be determined from the titration experiment shown in Figure 2 (*33*, *34*). Let us denote with n_P^o and c_P^o the total molar amount and the total concentration, respectively, of peptide in the calorimeter cell. After i injections of phospholipid vesicles, the mole fraction of bound peptide is

$$\theta_{P,b}^{(i)} = n_{P,b}^{(i)}/n_P^o = \sum_{k=1}^{i} \delta h_k / \Delta H V_{cell} c_P^o \qquad (3)$$

where $n_{P,b}^{(i)}$ is the molar amount of bound peptide after i injections, V_{cell} is the volume of the calorimeter cell, and ΔH is the molar enthalpy of binding. The free peptide concentration in the calorimeter cell after i injections can be calculated according to

$$c_{P,f}^{(i)} = c_P^o(1 - \theta_{P,b}^{(i)}) \qquad (4)$$

The amount of lipid in the cell increases with each injection and after i titration steps is given by

$$n_L^{(i)} = i V_{inj} c_L^o \qquad (5)$$

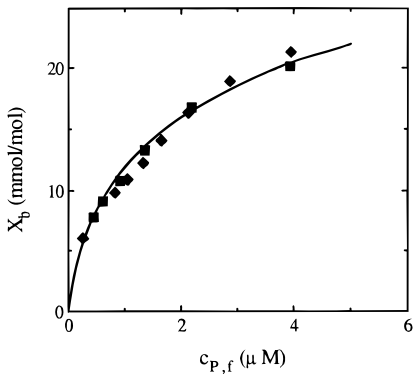

FIGURE 4: Binding isotherm of magainin 2 amide for small unilamellar vesicles ($d \sim 30$ nm diameter) as derived from titration calorimetry. The degree of binding, X_b (i.e., millimoles of peptide bound per mole of lipid), is plotted against the free (equilibrium) peptide concentration in bulk solution, $c_{P,f}$ ($T = 30$ °C). Lipid titrated into a peptide solution of concentration (◆) 5.36 μM of (■) 6.6 μM. The amount of bound peptide after "i" injection steps is proportional to $\sum_i \Delta h_i/\Delta H$, which can be translated into X_b and $c_{P,f}$. The solid line is the theoretical binding isotherm calculated by combining the Gouy−Chapman theory with a surface partition equilibrium using an intrinsic binding constant $K = 50$ M^{-1} and a peptide charge of $z = 3.7-3.8$. The latter was calculated with a variable pH at the membrane surface using a pK value of pK = 7.2 for the N-terminal amino group.

where c_L^o is the concentration of the lipid stock solution and V_{inj} the injected volume per titration step.

Knowledge of the bound peptide, $n_{P,b}^{(i)}$, and the total injected lipid, $n_L^{(i)}$, yields the degree of binding, $X_b^{(i)}$, defined as

$$X_b^{(i)} = n_{P,b}^{(i)}/n_L^{(i)} \tag{6}$$

The two essential parameters which constitute the binding isotherm, namely, the degree of binding, X_b, and the corresponding free peptide concentration, $c_{P,f}$, can thus be determined from a single titration experiment. This is shown in Figure 4 for two different titration experiments. The data points in Figure 4 correspond to the individual titration steps. The solid line was calculated with a theoretical binding model to be discussed in more detail below. It should be emphasized that the above derivation of the experimental binding isotherm is model-independent and does not require any specific theoretical assumptions. Apparent partition coefficients can be calculated directly from the binding isotherm according to $K_{app} = X_b/c_{P,f}$. In terms of this simple model, K_{app} will depend on the peptide concentration. Inspection of Figure 4 yields $K_{app} \approx 1.2 \times 10^4$ M^{-1} at a peptide equilibrium concentration of 1 μM with K_{app} decreasing at higher peptide concentrations.

Quantitative magainin binding data are scarce. Matsuzaki et al. and Wieprecht et al. employed CD spectroscopy to derive binding isotherms for different magainins (*11, 35*). The latter authors used conditions similar to those in the present experiment. Up to a concentration of $c_{P,f} \sim 1$ μM, the reported CD titration curve is in approximate agreement with the present data (~30% deviation). At larger peptide concentrations, the CD data have a biphasic appearance and are smaller than those obtained with titration calorimetry. The difference can probably be traced back to the much lower sensitivity of CD spectroscopy.

DISCUSSION

Magainin 2 amide (M2a) has four positive charges and one negative fixed charge. In addition, the N-terminal amino group is also partially positive with a p$K \sim 7.2$. The net charge of M2a is thus $3 \leq z \leq 4$ and will vary with the pH. The binding of the positively charged M2a to the negatively charged POPC/POPG membranes can be divided into at least two steps. The first step is an electrostatic adsorption process which leads to a distinctly increased peptide concentration immediately above the plane of the membrane. The second step is a hydrophobic adsorption which is characterized by penetration of the peptide into the lipid bilayer, be it only into the headgroup region, or even into the hydrophobic part of the lipid bilayer. The theoretical treatment for the binding of molecules with a fixed charge has been developed first for drug molecules and potential sensitive dyes (*36, 37*) and then for peptides such as melittin (*38, 39*) or pentalysin (*40*). More recently, the variation of the charge of the amino-terminal was also included in the calculation (*41*). This effect is relevant for membranes with a negative surface charge where the proton density and thus the pH vary with the distance from the membrane surface. Close to the membrane surface the proton density is higher and the pH lower than in bulk solution.

Magainin 2 Amide Binding Model. The binding of M2a to negatively charged membranes will be described in terms of the model proposed for somatostatin-like peptides (*41*). The essential elements of this model are as follows. The binding of M2a to the lipid membrane is described in terms of a surface partition equilibrium:

$$X_b^{(i)} = Kc_M \tag{7}$$

$X_b^{(i)}$ is the molar amount of peptide bound (after titration step i), K is the intrinsic (chemical) partition coefficient which is independent of electrostatic effects, and c_M is the interfacial concentration of M2a immediately above the lipid membrane. The interfacial concentration, c_M, is related to its equilibrium concentration in bulk solution, $c_{P,f}$, according to

$$c_M = c_{P,f} \exp(-zF_o\psi_o/RT) \tag{8}$$

where z is the signed electric charge of the peptide, F_o is the Faraday constant, and RT is the thermal energy. An analogous relation holds true for the proton concentration. The membrane surface potential, ψ_o, is not known a priori, but is related to the membrane surface charge density, σ, according to

$$\sigma^2 = 2000\epsilon_o\epsilon_r RT\sum c_{i,eq}(e^{-z_iF_o\psi_o/RT} - 1) \tag{9}$$

where $c_{i,eq}$ is the concentration of the ith electrolyte in the bulk aqueous phase, z_i the signed valency of the ith species, ϵ_o the electric permittivity of free space, ϵ_r the dielectric constant of water, and T the absolute temperature. The basic principles of the Gouy−Chapman theory have been discussed in a number of books and review articles (*37, 42, 43*). The surface charge density is then related to X_b which, in turn, is experimentally accessible from the calorimetric measurements.

Na^+ binding to POPG was included with a Na^+ binding constant of 0.6 M^{-1} and was assumed to follow a Langmuir

adsorption isotherm (*44*). The pK of the N-terminal amino group was assumed as pK = 7.2 (*45*). The pH at the membrane−water interface was calculated to be in the range of 6.6 < pH < 6.9, depending on the surface charge density σ. The partial charge of the N-terminal amino group varied according to the pH and was $\delta z_{NH_3^+} \approx 0.7-0.8$. Together with the fixed charge of $z = +3$, this led to a total effective charge of $z = 3.7-3.8$, depending on the pH at the membrane surface. The details of the theory have been described recently (*41*). The solid line in Figure 2B (Figure 3F−K; Figure 4)was calculated with this model, using a binding constant of $K = 50$ M^{-1} (60 M^{-1}; 60 M^{-1}) and a enthalpy value of $\Delta H = -17.0$ kcal/mol. For peptide concentrations below $c_P^o = 7$ μM, only M2a binding to the outer monolayer is considered. An excellent agreement between experimental and theoretical binding isotherms is obtained at low peptide concentrations (Figure 2, Figure 4).

Knowledge of the partition constant K allows the calculation of the chemical part of the free energy of binding according to $\Delta G = -RT$ ln(55.5 K), yielding $\Delta G = -4.8$ kcal/mol. The factor 55.5 corrects for the cratic contribution since the concentration of the peptide in solution is measured in moles per liter, and that in the membrane phase, however, in moles of peptide per mole of lipid (*46*). In view of the large negative reaction enthalpy of $\Delta H = -17$ kcal/mol, the binding of M2a to sonicated lipid vesicles appears to be enthalpy-driven, a phenomenon which has been termed 'non-classical' hydrophobic effect and has been observed also for other amphiphilic molecules and peptides (*47*−*50*). The intrinsic binding constant of M2a is not large and is comparable to that of somatostatin and its analogs (*41*) which are characterized by $K \approx 50$ M^{-1}. This suggests that M2a does not penetrate deeply into the hydrophobic interior of the membrane but remains bound superficially. This is in contrast to melittin, which is also an amphiphilic molecule but binds to POPC/POPG sonified vesicles with $K_p \approx 4.6 \times 10^4$ M^{-1} (*39*).

For practical applications, the overall binding constant K_{app} is often preferred since it includes both electrostatic and chemical effects. For the present system, K_{app} varies from $K_{app} \approx 1.2 \times 10^4$ M^{-1} for $c_{P,f} \approx 1.0$ μM to $K_{app} \approx 5 \times 10^3$ M^{-1} at $c_{P,f} \approx 5.0$ μM. A comparison of K and K_{app} demonstrates that the adsorption/binding of M2a to the lipid membrane is dominated by electrostatic attraction.

Magainin 2 Amide Pore Formation. For large M2a concentrations, spectroscopic measurements suggest a rapid flip-flop of the lipid molecules and a translocation of the peptide across the bilayer membrane (*14*, *27*). However, even with this modification (100% lipid availability), a simple partition model alone is no longer sufficient to describe the experimental titration curves above a critical limit of $c_P^o \approx 7$ μM (Figure 3). The deviations from the theoretical model increase with increasing peptide concentration. The experimental titration curves can be divided into three parts in which the experimental $|\delta h_i|$ values are either smaller, larger, or identical to $|\delta h_{theor}|$. The excess heat can be defined as

$$\delta H_{ex} = \sum_i (\delta h_{i,exp} - \delta h_{i,theor}) \qquad (10)$$

and can be evaluated for the different phases of the titration experiment. For the experiments shown in Figure 3F−I, these values amount to +25 μcal and −28 μcal (for the first and second part, respectively), +32/−36 μcal, +44/−46 μcal, and +156/−154 μcal, respectively. Within experimental error, the endothermic excess enthalpy of the first few injections is compensated by the exothermic excess enthalpy during the second part of the titration experiment. The experimental titration curves merge with the theoretical predictions only at very large lipid-to-peptide ratios.

A similar phenomenon has been observed recently for the titration of lipid vesicles into octyl glucoside solutions of sufficiently high surfactant concentration (*32*). The deviation from the theoretical prediction could be explained by a micellization ↔ demicellization phenomenon of the phospholipid vesicles. Such a process can, however, be excluded in the present investigation since light scattering data yield a constant scattering intensity of the phospholipid vesicles at all M2a concentrations. Instead we assign the excess enthalpies to a M2a pore formation ↔ pore disintegration equilibrium. CD spectroscopy indicates a random coil structure for magainin in buffered solution (*11*, *51*). Addition of negatively charged phospholipid induces a conformational transition toward an essentially α-helical structure. The orientation of the magainin helix with respect to the plane of the lipid membrane was investigated with oriented circular dichroism and NMR spectroscopy. At low peptide concentrations, the helices were found to lie parallel to the membrane surface (*20*, *22*, *23*, *26*). However, for peptide-to-lipid ratios P/L ∼1/30, a substantial fraction of the bound peptide adopted an orientation perpendicular to the membrane surface (*20*). The arrangement of the helix bundles was recently refined on the basis of neutron diffraction and fluorescence spectroscopy studies (*14*, *27*, *51*). In the high concentration regime, the helices form pores in which the individual helices are separated by lipids. In this model, the bilayer bends back on itself like the inside of a torus (*14*). The peptide−lipid complex is highly dynamic, and lipid molecules diffuse freely between the two monolayers through the perimeter of the pore (*27*).

The toroidal pore formation model can be used for a structural interpretation of the calorimetric data of Figure 3. The three stages of the calorimetric titration can be assigned to three distinct molecular processes. Partitioning of M2a into the lipid phase occurs during the whole titration experiment and produces an exothermic heat of reaction. However, additional enthalpies come into play due to M2a pore formation and pore disintegration. In the initial phase of the titration experiment, the P/L ratio in the calorimeter cell is high, and M2a partitioning is followed by M2a pore formation. Pore formation is an endothermic process. Based on the measured heat reduction observed in Figure 3 and the amount of peptide bound in the initial titration phase, the enthalpy of pore formation can be evaluated as $\Delta H = 6.2 \pm 1.6$ kcal/mol of peptide. If a pore is composed of 4−7 magainin monomers (*14*), the total enthalpy of pore formation is $\Delta H_{pore} \sim 25-45$ kcal per pore. The formation of M2a pores in the lipid membrane is thus enthalpically unfavorable and must be an entropy-driven process. With increasing lipid injections, the P/L ratio decreases, and pore formation comes to a halt. Addition of further lipid will shift the pore ↔ monomer equilibrium toward the M2a monomer phase, and the pore will disintegrate. The pore

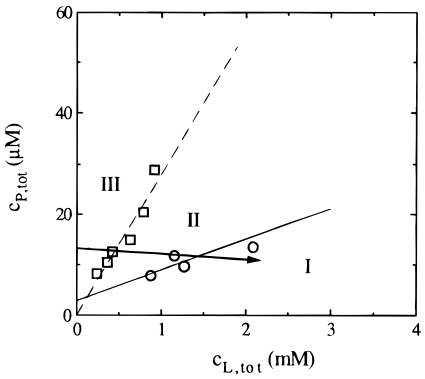

FIGURE 5: "Phase diagram" of pore formation of magainin 2 amide in aqueous mixtures with phospholipid vesicles composed of POPC and POPG (75:25, mol/mol) at 30 °C. The symbols denote the experimental discontinuities as determined from the experiments shown in Figure 3. The straight lines are the least-squares fits to the data. The dashed line has a slope of $m = 0.029$ (±0.004) and corresponds to a ratio of ~3.0 mol % of peptide to lipid. It marks the boundary between the pore region III and the coexistence region II of pores and monomers. The solid line marks the boundary between peptide monomers (region I) and the coexistence region. The arrow represents the direction of the titration experiment shown in Figure 3E.

disintegration is exothermic and will return the enthalpy consumed during pore formation. This explains the approximate symmetry of the positive and negative excess enthalpies as revealed by Figure 3. Finally, at very high L/P ratios, only monomers are found on the membrane surface, and the experimental results follow the theoretical partition model.

The thermodynamic data suggest a simple scheme to describe the M2a pore ↔ monomer equilibrium. To this purpose, Figure 5 shows a plot of the total peptide concentration, $C_{P,tot}$, vs the total lipid concentration, $C_{L,tot}$, derived from Figure 3 in the following manner. For a given peptide concentration, $C_{P,tot}$, those two lipid concentrations, $C_{L,tot}$, were determined where the experimental titration curve intersects the binding isotherm of the partition model. The dashed line then connects data points corresponding to high P/L ratios. It defines the boundary between pure pores (region III) and the coexistence region (region II). In the latter, pores and M2a monomers coexist at variable ratios. The solid line connects data points with a low P/L ratio and describes the boundary between the coexistence region II and the pure monomer region I. Region I is the simple partition equilibrium of M2a in solution, i.e., the equilibrium between a random-coil conformation in solution and M2a bound in helical conformation parallel to the membrane surface.

Linear regression analysis of the data in Figure 5 yields

$$c_{P,tot}(\mu M) \approx 0.85 + 0.029 c_{L,tot}(\mu M) \qquad (11)$$

for the boundary between the pore region and the coexistence region. All data points are characterized by the same $X_b = 21.3 \pm 1.2$ mmol/mol and $c_{p,f} = 4.4 \pm 0.7$ μM. The boundary between the pore/monomer coexistence region and the pure monomer region is given by

$$c_{P,tot}(\mu M) \approx 5.5 + 0.048 c_{L,tot}(\mu M) \qquad (12)$$

The boundaries derived by titration calorimetry are in agreement with spectroscopic data and with measurements of biological activity. At magainin concentrations >~3.3 mol %, CD spectroscopy showed that 50−100 % of the peptide was inserted perpendicular into the membrane (*14*, *20*), which is consistent with the boundary III/II defined by eq 11. On the other hand, ^{15}N solid-state NMR spectroscopy provides evidence for magainin 2 helices oriented parallel to the bilayer surface when the total magainin 2:lipid ratios are 0.8−3 mol % (*7*, *22*, *26*). Cytotoxicity studies revealed that 0.6−3 mol % magainin resulted in half-maximal decoupling of the respiratory free energy transduction in bacteria, isolated mitochondria, and reconstituted cytochrome *c* oxidase liposomes (*10*, *12*, *52*). In the present study, the concentration range of 0.8−3 mol % can be identified as the coexistence range of parallel and perpendicular helix orientations. Since the percentage of the two varies, the perpendicular orientation could have escaped notice in the NMR experiments. It should also be noted that Figure 5 is valid for sonified, 30 nm lipid vesicles composed of POPC/POPG (3:1) whereas most of the previous CD, NMR, and neutron diffraction studies employed oriented planar bilayers squeezed between quartz plates. The lateral packing density of the lipids is higher in planar than in highly curved unilamellar vesicles. In addition, lipids with saturated fatty acyl chains were employed in most of the earlier studies. Both factors together could shift the boundaries toward slightly higher magainin 2 concentrations than observed in Figure 5.

CONCLUSIONS

We have used high-sensitivity titration calorimetry to investigate the binding of magainin 2 amide to sonified phospholipid vesicles composed of POPC and POPG (75:25 mol/mol). The binding process can be described quantitatively by a surface partition equilibrium amplified by strong electrostatic attraction. The partition coefficient after correction for electrostatic effects is $K = 55 \pm 5$ M^{-1}, the enthalpy of binding is $\Delta H = -17 \pm 1$ kcal/mol, and the effective charge of the peptide is $z \approx 3.7-3.8$, depending on the pH at the membrane surface and the extent of protonation of the terminal amino group. The binding of M2a is caused essentially by electrostatic forces. The overall binding constant, K_{app}, which includes both hydrophobic and electrostatic contributions, varies considerably between ~10^5 M^{-1} and 10^3 M^{-1} (and lower) depending on the peptide concentration, the membrane surface charge, the salt concentration, and other experimental conditions. At high peptide concentrations, excess enthalpies were observed which are assigned to an insertion of the helical peptide into the lipid membrane followed by pore formation. Pore formation is enthalpically unfavorable and requires $\Delta H = 6.2 \pm 1.6$ kcal/mol peptide or $\Delta H \approx 25-45$ kcal/mol pore if the pore is composed of 4−7 peptides.

ACKNOWLEDGMENT

We thank W. Lee Maloy, Magainin Pharmaceuticals, Inc. (Plymouth Meeting, PA), for his generous gift of magain 2 amide and constructive comments.

REFERENCES

1. Zasloff, M., Martin, B., and Chen, H. C. (1988) *Proc. Natl. Acad. Sci. U.S.A. 85*, 910−913.

2. Zasloff, M. (1987) *Proc. Natl. Acad. Sci. U.S.A. 84*, 5549−5553.
3. Cruciani, R. A., Barker, J. L., Zasloff, M., Chen, H. C., and Colamonici, O. (1991) *Proc. Natl. Acad. Sci. U.S.A. 88*, 3792−3796.
4. Soballe, P. W., Maloy, W. L., Myrga, M. L., Jacob, L. S., and Herlyn, M. (1995) *Int. J. Cancer 60*, 280−284.
5. Segrest, J. P., De Loof, H., Dohlman, J. G., Brouillette, C. G., and Anantharamaiah, G. M. (1990) *Proteins: Struct., Funct., Genet. 8*, 103−117.
6. Segrest, J. P., Garber, D. W., Brouillette, C. G., Harvey, S. C., and Anantharamaiah, G. M. (1994) *Adv. Protein Chem. 45*, 303−369.
7. Bechinger, B. (1997) *J. Membr. Biol. 156*, 197−211.
8. Saberwal, G., and Nagaraj, R. (1994) *Biochim. Biophys. Acta 1197*, 109−131.
9. Epand, R. M., Shai, Y., Segrest, J. P., and Anantharamaiah, G. M. (1995) *Biopolymers 37*, 319−338.
10. Westerhoff, H. V., Juretic, D., Hendler, R. W., and Zasloff, M. (1989) *Proc. Natl. Acad. Sci. U.S.A. 86*, 6597−6601.
11. Matsuzaki, K., Harada, M., Funakoshi, S., Fujii, N., and Miyajima, K. (1991) *Biochim. Biophys. Acta 1063*, 162−170.
12. Juretic, D., Hendler, R. W., Kamp, F., Caughey, W. S., Zasloff, M., and Westerhoff, H. V. (1994) *Biochemistry 33*, 4562−4570.
13. Matsuzaki, K., Sugishita, K., Fujii, N., and Miyajima, K. (1995) *Biochemistry 34*, 3423−3429.
14. Ludtke, S. J., He, K., Heller, W. T., Harroun, T. A., Yang, L., and Huang, H. W. (1996) *Biochemistry 35*, 13723−13728.
15. Dathe, M., Wieprecht, T., Nikolenko, H., Handel, L., Maloy, W. L., MacDonald, D. L., Beyermann, M., and Bienert, M. (1997) *FEBS Lett. 403*, 208−212.
16. Matsuzaki, K., Harada, M., Handa, T., Funakoshi, S., Fujii, N., Yajima, H., and Miyajima, K. (1989) *Biochim. Biophys. Acta 981*, 130−134.
17. Grant, E., Jr., Beeler, T. J., Taylor, K. M., Gable, K., and Roseman, M. A. (1992) *Biochemistry 31*, 9912−9918.
18. Cruciani, R. A., Barker, J. L., Durell, S. R., Raghunathan, G., Guy, H. R., Zasloff, M., and Stanley, E. F. (1992) *Eur. J. Pharmacol. 226*, 287−296.
19. Duclohier, H. (1994) *Toxicology 87*, 175−188.
20. Ludtke, S. J., He, K., Wu, Y., and Huang, H. W. (1994) *Biochim. Biophys. Acta 1190*, 181−184.
21. Bechinger, B., Kim, Y., Chirlian, L. E., Gesell, J., Neumann, J. M., Montal, M., Tomich, J., Zasloff, M., and Opella, S. J. (1991) *J. Biomol. NMR 1*, 167−173.
22. Bechinger, B., Zasloff, M., and Opella, S. J. (1992) *Biophys. J. 62*, 12−14.
23. Hirsh, D. J., Hammer, J., Maloy, W. L., Blazyk, J., and Schaefer, J. (1996) *Biochemistry 35*, 12733−12741.
24. Williams, R. W., Starman, R., Taylor, K. M., Gable, K., Beeler, T., Zasloff, M., and Covell, D. (1990) *Biochemistry 29*, 4490−4496.
25. Matsuzaki, K., Murase, O., Tokuda, H., Funakoshi, S., Fujii, N., and Miyajima, K. (1994) *Biochemistry 33*, 3342−3349.
26. Bechinger, B., Zasloff, M., and Opella, S. J. (1993) *Protein Sci. 2*, 2077−2084.
27. Matsuzaki, K., Murase, O., Fujii, N., and Miyajima, K. (1996) *Biochemistry 35*, 11361−11368.
28. Matsuzaki, K., Nakamura, A., Murase, O., Sugishita, K., Fujii, N., and Miyajima, K. (1997) *Biochemistry 36*, 2104−2111.
29. Nebel, S., Ganz, P., and Seelig, J. (1997) *Biochemistry 36*, 2853−2859.
30. Wiseman, T., Williston, S., Brandts, J. F., and Lin, L. N. (1989) *Anal. Biochem. 179*, 131−137.
31. Wenk, M. R., Alt, T., Seelig, A., and Seelig, J. (1997) *Biophys. J. 72*, 1719−1731.
32. Wenk, M. R., and Seelig, J. (1997) *J. Phys. Chem. B 101*, 5224−5231.
33. Beschiaschvili, G., and Seelig, J. (1991) *Biochim. Biophys. Acta 1061*, 78−84.
34. Seelig, J. (1997) *Biochim. Biophys. Acta 1331*, 103−116.
35. Wieprecht, T., Dathe, M., Schumann, M., Krause, E., Beyermann, M., and Bienert, M. (1996) *Biochemistry 35*, 10844−10853.
36. McLaughlin, S., and Harary, H. (1976) *Biochemistry 15*, 1941−1948.
37. McLaughlin, S. (1977) *Curr. Top. Membr. Transp. 9*, 71−144.
38. Kuchinka, E., and Seelig, J. (1989) *Biochemistry 28*, 4216−4221.
39. Beschiaschvili, G., and Seelig, J. (1990) *Biochemistry 29*, 52−58.
40. Kim, J., Mosior, M., Chung, L. A., Wu, H., and McLaughlin, S. (1991) *Biophys. J. 60*, 135−148.
41. Seelig, J., Nebel, S., Ganz, P., and Bruns, C. (1993) *Biochemistry 32*, 9714−9721.
42. Aveyard, R., and Haydon, D. A. (1973) *An Introduction to the Principles of Surface Chemistry*, Cambridge University Press, London.
43. McLaughlin, S. (1989) *Annu. Rev. Biophys. Biophys. Chem. 18*, 113−116.
44. Macdonald, P. M., and Seelig, J. (1987) *Biochemistry 26*, 1231−1240.
45. Seelig, A. (1990) *Biochim. Biophys. Acta 1030*, 111−118.
46. Cantor, C. R., and Schimmel, P. R. (1980) in *Biophysical Chemistry*, p 145, Freeman, San Francisco.
47. Seelig, J., and Ganz, P. (1991) *Biochemistry 30*, 9354−9359.
48. Beschiaschvili, G., and Seelig, J. (1992) *Biochemistry 31*, 10044−10053.
49. Terzi, E., Holzemann, G., and Seelig, J. (1994) *Biochemistry 33*, 7434−7441.
50. Wenk, M. R., Fahr, A., Reszka, R., and Seelig, J. (1996) *J. Pharm. Sci. 85*, 228−231.
51. Wieprecht, T., Dathe, M., Beyermann, M., Krause, E., Lee Maloy, W., MacDonald, D. L., and Bienert, M. (1997) *Biochemistry 36*, 6124−6132.
52. Westerhoff, H. V., Hendler, R. W., Zasloff, M., and Juretic, D. (1989) *Biochim. Biophys. Acta 975*, 361−369.

BI972615N